Research Article Vol. 34, No. 8 / 20 Apr 2026 / Optics Express 14465
Optics EXPRESS

Directly modulated lasers with graded-κ grating for stable single-mode operation and bandwidth enhancement

YOUNGHOON KIM,[1,†] SEOK-JUN YUN,[1,†] YOUNG-TAK HAN,[1] SANG-HO PARK,[1] SHINMO AN,[1] YOUNG AHN LEEM,[1] HONGSIK PARK,[2] HONGHWI PARK,[1,3,4] AND DONG-HOON LEE[1,5]

[1] *Photonic/Wireless Devices Research Division, Electronics and Telecommunications Research Institute (ETRI), Daejeon 34129, Republic of Korea*
[2] *School of Electronic and Electrical Engineering, Kyungpook National University, Daegu 41566, Republic of Korea*
[3] *School of Electronic Engineering, Kumoh National Institute of Technology, Gumi-si, Gyeongbuk 39177, Republic of Korea*
[4] *hp@kumoh.ac.kr*
[5] *dhlee@etri.re.kr*
[†] These authors equally contributed to this work.

Abstract: We present a graded-κ grating technique that enables stable single-mode lasing and robust modulation-bandwidth enhancement in directly modulated lasers. Internal reflection at the interface between the active and passive regions typically degrades detuned-loading and photon–photon resonance effects, which limit high-speed operation. The proposed graded-κ structure suppresses these reflections by smoothing the photon-density and refractive-index transition, resulting in fluctuation-free bandwidth scaling and reliable activation of single-cavity etalon effects. The device achieves a 3-dB bandwidth of 47.5 GHz and supports 112-Gbps PAM4 transmission with TDECQ values lower than 2.9 dB up to 45 °C, demonstrating its suitability for next-generation optical interconnect solutions in datacenters.

1. Introduction

In recent years, the rapid advancement of cloud computing, artificial intelligence, and big-data technologies has led to an explosive growth in global data traffic. This trend has created an unprecedented demand for optical communication systems featuring high speed, low latency, and high channel density. To meet these requirements, 400-Gbps and 800-Gbps optical modules based on 100-Gbps-per-lane architectures have been widely deployed in datacenter networks. Moreover, 200-Gbps-per-lane pulse amplitude modulation with four levels (PAM4) is emerging as a key technology for next-generation Ethernet systems. As a critical building block for realizing such high-speed modules, optical transmitters with high modulation bandwidth and channel density are strongly required [1]. Among various transmitter technologies, electro-absorption modulated lasers [2–6], thin-film lithium niobate modulators, silicon photonics, and directly modulated lasers (DMLs) [7–9] have been extensively investigated. Compared with other transmitter schemes employing external modulators or separate light sources, DMLs offer several compelling advantages including simple device fabrication, compact footprint, low power consumption, and cost effectiveness. These features make DMLs particularly attractive for high-speed and low-cost optical interconnect solutions in datacenters. To support higher data transmission rates, DMLs must exhibit sufficiently high modulation bandwidth. However, conventional DMLs suffer from intrinsic performance limitations imposed by the relaxation oscillation frequency, damping factor, and RC time delay. These factors typically restrict the 3-dB modulation bandwidth to

#587817 https://doi.org/10.1364/OE.587817
Journal © 2026 Received 17 Dec 2025; revised 10 Mar 2026; accepted 29 Mar 2026; published 9 Apr 2026

Optics EXPRESS

approximately 30 GHz under standard operating conditions, making it challenging to achieve the bandwidth required for next-generation high-speed transmission formats such as 200-Gbps PAM4 [8,10,11].

To overcome the bandwidth limitations of conventional DMLs, various bandwidth-enhancement techniques based on detuned-loading effects [12,13] and photon–photon resonance (PPR) effects [14,15] have been actively investigated. To induce these effects, DML device schemes integrating short distributed feedback (DFB) active section with a distributed Bragg reflector (DBR) or a passive waveguide coated with a low-reflectivity facet have been demonstrated, and these schemes enable modulation bandwidths exceeding 45 GHz while maintaining stable single-mode operation and sufficient optical output power [15–19]. Among the reported DML structures exploiting detuned-loading and PPR effects, the DFB active section integrated with a low-reflectivity passive waveguide (referred to as 'DFB + R' laser) has been particularly considered as a promising and practical architecture for emerging optical transmitters. This is attributed to its high fabrication yield, simple device/process design, cost-effectiveness, high power/speed at low bias, compact footprint, low chirp, and isolator-free operation [15]. To maximize the detuned-loading and PPR effects in DFB + R lasers, a passive waveguide coated with a few-% reflectivity facet is essentially integrated with the DFB active section and serves as the output facet. Increasing the reflectivity of the passive-waveguide facet enhances the optical feedback strength and induces the changes in feedback phase, both of which are beneficial for inducing detuned-loading and PPR effects. However, excessive reflectivity coating on the passive-waveguide facet can cause phase mismatch and a reduction in optical output power, thereby necessitating an appropriate design trade-off; in this regard, a reflectivity of approximately 3% has been reported as an optimal coating value for balancing modulation bandwidth and optical power in DML performance [15]. Such low-reflectivity facet configurations are therefore widely employed in practical DML transmitters to realize unidirectional emission and external-cavity–assisted bandwidth enhancement, although they may slightly decrease the side-mode suppression ratio compared to near-zero-reflectivity anti-reflection-coated facet configurations.

To achieve stable induction of these effects, however, it is necessary not only to optimize the reflectivity coating at the output facet but also to consider the internal reflection occurring at the butt-joint coupling interface between the DFB active section and the passive waveguide. Additional internal reflection can originate from the abrupt change in photon density at the butt-joint interface where DFB grating is terminated, which results in an effective refractive-index discontinuity. Consequently, two Fabry–Pérot (FP) etalon resonances would be formed in this structure: (i) the main FP etalon between the high-reflection (HR)-coated rear DFB facet and the few-%-coated front waveguide facet, and (ii) an additional etalon between the HR-coated rear facet and the butt-joint interface. This internal reflection induces a multiple-cavity effect, which can severely degrade the bandwidth enhancement achieved through the detuned-loading effect, since its mechanism relies on precise control of the detuning between the lasing mode and the adjacent FP etalon modes. As a result, both the single-mode yield and the modulation performance can be degraded; hence, effective suppression of internal reflection at the butt-joint interface is essential for achieving stable modulation bandwidth enhancement. However, in-depth studies addressing this issue in high-speed DMLs still remain limited. In this work, we introduce a graded-kappa (κ) grating that suppresses internal reflection and spatial hole burning by mitigating the changes in refractive index and photon density near the butt-joint interface, and enables stable single-mode lasing operation, thereby effectively inducing both detuned-loading and PPR effects. Based on this approach, we present the experimental demonstration of PAM4 operation using the proposed high-speed DML, capable of supporting data rates exceeding 100 Gbps.

2. Device structure and fabrication

Figure 1(a) shows a schematic of the 1.3-μm O-band DFB + R laser diode (LD), in which a grating-based DFB active section is integrated with an InGaAsP passive waveguide section. The epitaxial structure of the active region consists of 8 pairs of compressively strained InAlGaAs multi-quantum wells (MQWs), embedded in separated-confinement heterostructure (SCH) layers. After the growth of the MQW and SCH layers using metal-organic chemical vapor deposition (MOCVD), an 80-nm-thick Zn-doped InGaAsP layer with a bandgap wavelength of 1.15 μm (*i.e.*, 1.15Q) was grown to serve as the grating layer. Using the grown epitaxial wafer, a uniform grating was first patterned by electron-beam lithography, followed by reactive-ion etching (RIE) to define the periodic DFB structure designed for a Bragg wavelength of 1.3 μm. Subsequently, the passive waveguide section was formed by patterning and etching using photolithography and an inductively-coupled-plasma RIE system, respectively. Afterward, a second MOCVD regrowth process was performed to selectively grow a 350-nm-thick InGaAsP layer (1.15Q) on the passive waveguide section. Following the formation of the ridge waveguides through 1.5-μm-wide MESA patterning and etching, additional MOCVD regrowth processes were sequentially carried out to grow the *p–n–p* InP current-blocking layers, the upper cladding layer with a Zn-doped *p*-InP layer, and a heavily Zn-doped InGaAs contact layer (2×10^{19} cm^{-3}) for ohmic contacts. Device surface passivation was then performed using a SiN film deposited by a plasma-enhanced chemical vapor deposition system, followed by contact opening. For metallization, Ti/Pt/Au metal stacks for the *p*-contacts were patterned by photolithography using a negative-tone photoresist and formed by a lift-off process, with ohmic behavior achieved through post-deposition rapid thermal annealing at 425 °C for 30 s. To improve heat dissipation and facilitate high-frequency probing, 3-μm-thick Au pads were electroplated onto the metal contacts, along with benzocyclobutene interlayers for reducing device capacitance. After epitaxial growth and LD device fabrication, the substrate was thinned down to about 100 μm using a mechanical lapping and polishing system, and then cleaved into chip bars with a cavity length of 250 μm using a scribing/cleaving machine.

Figure 1(b) displays the plan-view scanning electron microscope (SEM) image of the fabricated DFB + R laser, indicating that the DFB active section and the passive waveguide section are integrated through butt-joint coupling formed by the selective-area regrowth processes. It is noted that a slightly tilted butt-joint interface is observed between the InAlGaAs active region and the InGaAsP passive waveguide [inset of Fig. 1(b)], which helps minimize structural reflections at the interface. Figure 1(c) shows the cross-sectional SEM image of the DFB + R laser. It is confirmed that both the DFB MQW active and passive waveguides are formed as a buried heterostructure surrounded by *p–n–p* InP current-blocking layers, which enhances optical confinement and increases the relaxation oscillation frequency. It is noted that, in order to reduce the parasitic capacitance caused by the *p–n–p* InP current-blocking layers, trenches were formed on both sides of the waveguide to realize a narrow etched-MESA structure. In the fabricated device, the waveguide width is 3 μm, achieving a parasitic capacitance of approximately 1 pF. Figure 1(d) summarizes the overall schematic of the fabricated conventional DFB + R laser structure incorporating a quarter-wavelength (λ/4) shifter [20–22]. The total cavity length is 250 μm, consisting of a 130-μm-long DFB active LD section and a 120-μm-long passive waveguide section. The cleaved facet of the DFB active section is coated with a HR film, while the passive waveguide facet is coated with a 3% anti-reflection (AR) film. It is also shown that the λ/4 shifter is asymmetrically positioned toward the HR-coated side with a length ratio of 3:7, which was intentionally adopted to suppress spatial hole burning and ensure stable single-mode lasing even under high-current injection [20]. The lasing performance characteristics of the fabricated conventional DFB + R laser with the butt-joint interface between the uniform-grating DFB section and the passive waveguide section will be discussed in Fig. 2.

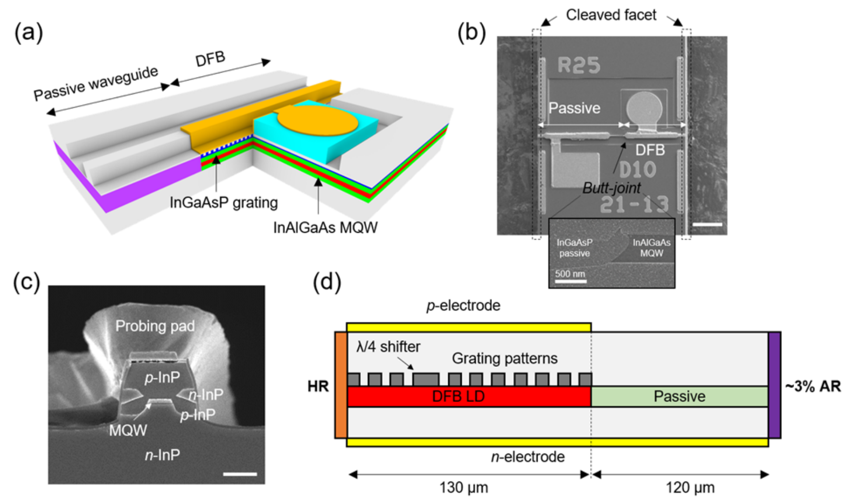

Fig. 1. (a) Schematic of the DFB + R directly modulated laser diode, integrated with a grating-based DFB section on InAlGaAs MQW and a passive waveguide section on InGaAsP. (b) Plan-view SEM image of the fabricated DFB + R laser, showing butt-joint coupling between the DFB LD section and the passive waveguide section. Scale bar is 50 µm. *Inset*: Cross-sectional SEM image of the butt-joint interface between the InAlGaAs active and the InGaAsP passive. (c) Cross-sectional SEM image of the fabricated DFB + R laser. A buried heterostructure with a *p–n–p* InP current-blocking layer is employed to enhance optical confinement and relaxation oscillation frequency. The scale bar is 2 µm. (d) Schematic of the conventional DFB + R laser structure with quarter-wavelength (λ/4) shifter, where the cleaved facet of the DFB LD section is coated with a HR film while the passive waveguide facet is coated with a low-reflectivity (~3%) AR film.

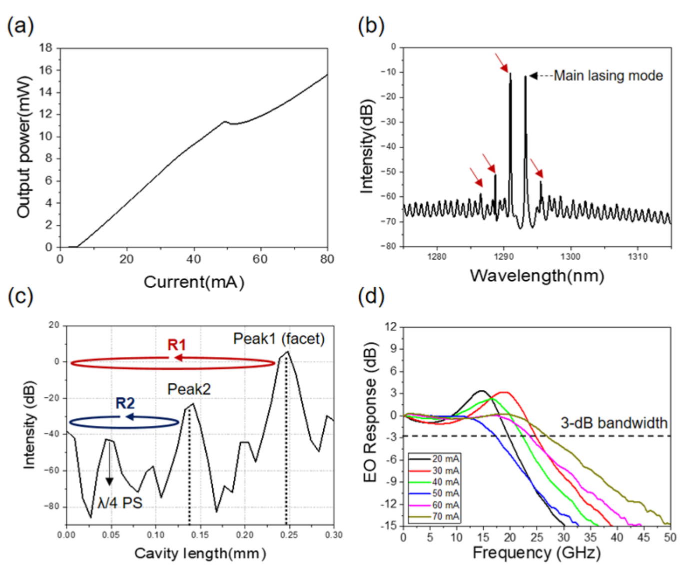

Fig. 2. Lasing and bandwidth characterizations of the fabricated DFB + R laser with uniform grating. (a) *L–I* characteristics and (b) optical spectrum, showing the undesirable multi-mode behaviors at a high current operation. (c) FFT-transformed light intensity of the optical spectrum, indicating two distinct peaks and a resonant etalon along the cavity length originating from the facet and the LD/passive interface. (d) Small-signal EO frequency responses of the fabricated uniform-grating DFB + R laser, measured at 25 °C.

3. Results and discussion

3.1. Performance characteristics of DFB + R lasers with uniform and graded-κ grating

Figure 2(a) shows the light–current (*L–I*) characteristics of the fabricated DFB + R laser with uniform-grating DFB under continuous-wave (CW) operation. A clear mode-hopping behavior is observed when the injection current exceeds approximately 50 mA. Figure 2(b) presents the corresponding optical spectrum measured near 50 mA. Despite the incorporation of an asymmetric λ/4 phase shifter, undesirable multi-mode lasing is observed within the stopband. This behavior is attributed to internal reflection occurring near the butt-joint interface at the end of the DFB section, which originates from the abrupt change in photon density and effective refractive index. The presence of internal reflection is further verified by the fast Fourier transform (FFT) of the optical spectrum, as shown in Fig. 2(c). Two dominant reflection peaks are clearly identified: a strong reflection R1 at approximately 250 µm, corresponding to the cleaved facet, and an additional reflection R2 at approximately 130 µm, corresponding to the butt-joint interface. These results indicate that two FP etalon resonances are simultaneously formed along the cavity: (i) between the HR-coated rear DFB facet and the 3%-coated front passive-waveguide facet, and (ii) between the HR-coated rear facet and the butt-joint interface. These internal reflections induce a multiple-cavity effect caused by the superposition of R1 and R2, which leads to unstable lasing modes accompanied by undesirable multi modes, as confirmed by Fig. 2(a) and Fig. 2(b). Figure 2(d) shows the small-signal electrical-to-optical (EO) frequency response of the DFB + R laser with the uniform grating, measured at 25 °C. The 3-dB modulation bandwidth initially increases with current up to approximately 30 mA, then decreases to about 17.5 GHz in the range of 40–50 mA, and subsequently increases again to 27.2 GHz at 70 mA. Notably, no significant modulation bandwidth enhancement attributed to detuned-loading or PPR effects is observed. In our experimental investigations, this behavior was observed in approximately 75% of the DML devices within the fabricated chip. These results indicate that the multiple-cavity effect caused by internal reflections is highly detrimental to the activation of detuned-loading and PPR effects, resulting in degraded single-mode lasing stability and a reduced bandwidth-enhancement yield (see details in Fig. S1, Supplement 1).

To address this issue, we propose a graded-κ grating to mitigate the abrupt changes in photon density and effective refractive index at the butt-joint interface between the DFB LD active and the passive waveguide, as illustrated in Fig. 3(a). In the designed DFB + R laser with the graded-κ grating, the DFB and passive waveguide sections are likewise integrated using butt-joint coupling, and the dimensions of each section are identical to those in the conventional DFB + R laser with the uniform grating. However, at the end of the DFB section, a 9-µm-long graded-κ grating is introduced to extend toward the passive waveguide region. The graded-κ grating is designed such that the coupling coefficient (*i.e.*, grating strength) is gradually decreased in three steps, from 100 cm^{-1} to 70, 50, 30 cm^{-1} in the DFB LD section, and finally 0 cm^{-1} in the passive waveguide section, as shown in Fig. 3(b). The design details of the uniform and graded-κ gratings are summarized in Table 1. A grating period of 200 nm was adopted to obtain a Bragg wavelength near 1.3 µm, and this period was identically applied to both the uniform and graded-κ regions. To realize the target grating-strength (κ) values, the fill factor of the InGaAsP grating in each graded-κ section was designed on the basis of the structural effective refractive index obtained from FDTD mode simulations. Using the square-grating relation, $\kappa = 2\Delta n_{\text{eff}}/\lambda$, the fill factor was swept so that the effective index differences required for the target κ values of 70, 50, and 30 cm^{-1} could be satisfied. As a result, when the fill factor is 0.38, 0.32, and 0.25, the corresponding effective indices are 3.2312, 3.2299, and 3.2286 for target κ values of 70, 50, and 30 cm^{-1}, respectively. Considering that the effective refractive index of the uniform grating is 3.2331 and that of the passive waveguide is 3.2266 at a wavelength of 1.3 µm, the structural effective refractive index under passive conditions (*i.e.*, without current

Optics EXPRESS

injection) also exhibits a gradual transition from the uniform-grating active region to the passive waveguide when the 3-stage graded-κ grating is introduced. More importantly, by progressively lowering the κ value near the LD/passive butt-joint interface, the graded-κ grating can suppress spatial hole burning and smooths the photon-density and effective-index distributions during laser operation. Consequently, internal reflections arising from the butt-joint interface can be effectively suppressed.

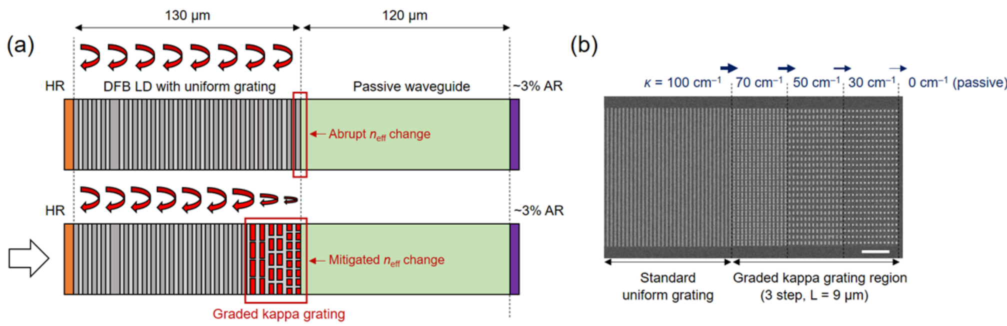

Fig. 3. (a) A schematic of the proposed DFB + R laser design with a graded-κ grating. By gradually lowering the kappa value near the LD/passive interface, internal reflections within the cavity can be mitigated by suppressing spatial hole burning and further minimizing abrupt changes in photon density and effective refractive index. (b) The fabricated 3-step graded-κ grating, in which the designed kappa value of the grating decreases progressively from 100 cm^{-1} to 70, 50, 30 cm^{-1} (DFB LD section), and finally 0 cm^{-1} (passive waveguide section). Scale bar is 1.5 µm.

Table 1. Design parameters of the uniform and graded-κ gratings in the DFB section

	DFB on MQW			
	Uniform grating	1st graded-κ grating	2nd graded-κ grating	3rd graded-κ grating
Grating period (nm)	200	200	200	200
Grating strength, k (cm^{-1})	100	70	50	30
Fill factor for InGaAsP grating	0.50	0.38	0.32	0.25
Grating-section length (µm)	121	3	3	3

Figure 4(a) shows the L–I characteristics of the proposed DFB + R laser with the graded-κ grating under CW operation. The threshold current is approximately 6 mA, and the optical output power increases linearly up to about 64 mA, beyond which a pronounced kink is observed. This type of kink is typically associated with mode hopping induced by the detuned-loading and PPR effects. Figure 4(b) shows the optical spectrum measured near 64 mA. Compared with the conventional DFB + R laser with a uniform grating, the graded-κ grating DFB + R exhibits stable single-mode lasing with a side-mode suppression ratio exceeding 50 dB within the stopband. This improvement is attributed to the effective suppression of internal reflection by the graded-κ grating, as verified by the FFT-transformed optical spectrum in Fig. 4(c). Only a single dominant reflection peak R1 is observed at the end of the cavity length of 250 µm, which corresponds to the main FP etalon formed between the HR-coated rear DFB facet and the 3%-coated front passive-waveguide facet. The absence of additional reflection peaks confirms that the laser can operate in a stable single-mode regime. This result further indicates that, in the graded-κ device, the high-current kink clearly corresponds to the controlled activation of the PPR/detuned-loading effects after suppression of the additional cavity, whereas the kink behavior

Optics EXPRESS

observed in the *L–I* characteristics of the uniform-grating device [Fig. 2(a)] is associated with multiple-cavity-induced unstable multi-mode lasing caused by residual internal reflection near the butt-joint interface. Figure 4(d) shows the room-temperature small-signal EO frequency response of the proposed DFB + R with the graded-κ grating. While the typical 3-dB modulation bandwidth of conventional all-active DMLs is limited to approximately 30 GHz, the modulation bandwidth of the proposed structure stably exceeds 35 GHz at injection currents above 50 mA due to the detuned-loading effect, and is further extended up to 47.5 GHz at a current of about 64 mA due to the PPR effect. In our experimental investigations, this modulation-bandwidth enhancement induced by detuned-loading and PPR was observed in more than 80% of the DML devices within the fabricated chip. These results indicate that the graded-κ grating effectively suppresses internal reflection and spatial hole burning by mitigating abrupt variations in refractive index and photon density near the butt-joint interface, thereby ensuring both stable single-mode lasing and robust modulation bandwidth enhancement induced by the detuned-loading and PPR effects. It should be also noted that the modulation bandwidth decreases noticeably immediately after the kink (@ bias current of > 66 mA) in the *L–I* curve in Fig. 4(a). This is because mode hopping shifts the main lasing mode to a different position within the reflection profile. As a result, the bandwidth-enhancement condition established before the kink is no longer maintained, and the modulation bandwidth decreases. Additional details regarding the bandwidth enhancement achieved by the proposed DFB + R with graded-κ grating are provided in Fig. S1 of Supplement 1.

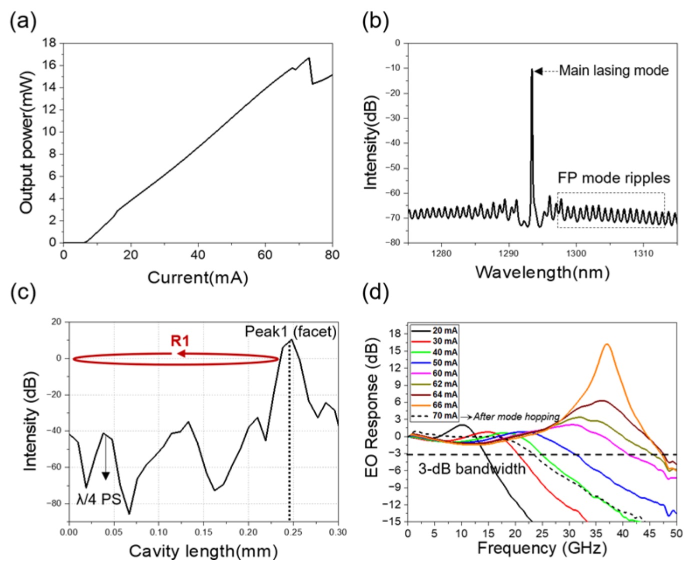

Fig. 4. Lasing and bandwidth characterizations of the fabricated DFB + R laser with a graded-κ grating. (a) *L–I* characteristics and (b) optical spectrum, showing stable single-mode operation. The kink in the *L–I* plot indicates mode hopping caused by the PPR and detuned loading effects. (c) FFT-transformed light intensity of the optical spectrum, indicating noticeable single peak and a Fabry–Pérot etalon between the laser facets. (d) Small-signal EO frequency responses of the fabricated graded-κ DFB + R laser, measured at 25 °C.

3.2. Dynamic performance characteristics of the proposed DFB + R laser

Figure 5(a) compares the 3-dB EO bandwidths of the DFB + R lasers with the uniform grating and the graded-κ grating, corresponding to the measurement results shown in Fig. 2 and Fig. 4, respectively. The black markers represent the DFB + R laser with the graded-κ grating, whereas the red markers denote the laser with the uniform grating. The 3-dB bandwidth of the graded-κ

Optics EXPRESS

grating DFB + R laser increases linearly with injection current up to 50 mA without noticeable fluctuations. This stable behavior is attributed to the effective suppression of internal reflection by the graded-κ grating. Beyond 50 mA, the EO bandwidth abruptly increases to 40.8 GHz at 60 mA due to the onset of the PPR effect and reaches a maximum value of 47.5 GHz at 64 mA. In contrast, the DFB + R laser with the uniform grating exhibits a normal bandwidth increase in the low-current region (20–30 mA), followed by a reduction in the mid-current range (30–50 mA). This degradation originates from internal reflections at the butt-joint interface between the DFB active section and the passive waveguide section. At higher injection currents (50–70 mA), the EO bandwidth increases again as the carrier density rises, leading to an enhancement of the relaxation oscillation frequency, but it gradually saturates as thermal chirp becomes more pronounced.

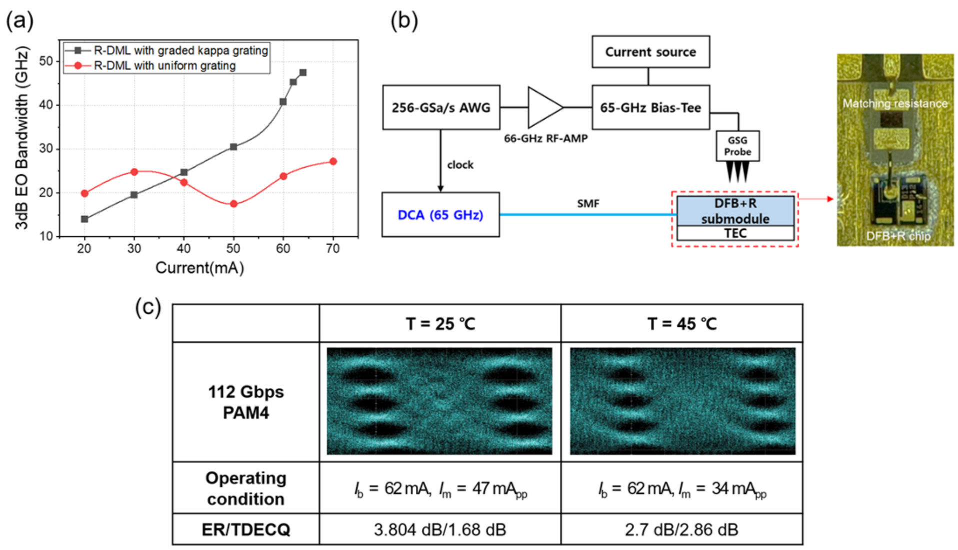

Fig. 5. LD dynamic characterizations. (a) 3-dB bandwidth comparison of the DFB + R lasers with uniform and graded-κ grating. Unlike the uniform-grating laser, the 3-dB bandwidth of the graded-κ grating laser steadily extends with increasing injection current, attributed to the PPR and detuned loading effects. (b) An experimental set-up for measuring eye diagrams. (c) The measured optical eye diagrams of the graded-κ grating DFB + R laser for a 112 Gbit/s PAM4 signal at 25 and 45 °C.

Figure 5(b) illustrates the experimental set-up used for eye diagram measurements. Data modulation experiments were performed using a packaged DFB + R laser submodule. The devices were mounted on a CuW sub-mount, where die bonding and wire bonding were employed to integrate the DFB + R laser, a 40-Ω surface-mount device (SMD) resistor, and a RF flexible printed circuit board (FPCB). The SMD resistor served as an impedance-matching component to ensure signal integrity at high frequencies. A ground–coplanar waveguide-type RF-FPCB was aligned and bonded to the CuW sub-mount to enable high-speed RF interconnection. Wire bonds were used to deliver both RF signals and bias currents to the DML. This submodule configuration minimizes parasitic effects and provides stable electrical and optical characteristics suitable for high-speed direct modulation [23].

To generate the PAM4 driving signals, a high-speed 256-GSa/s arbitrary waveform generator (AWG, Keysight M8199A) was used to produce 112-Gbps PAM4 signals. The output signal from the AWG was subsequently amplified by a linear RF amplifier with a 66-GHz bandwidth and a 22-dB gain, allowing the peak-to-peak driving current to be adjusted up to around 50

mA_{pp} assuming 50-Ω load. The amplified signal was fed into the DFB + R laser submodule through a ground–signal–ground (GSG) RF probe. The operating temperature of the DFB + R laser submodule was stabilized using a thermoelectric cooler. The modulated optical PAM4 signal was coupled into a lensed single-mode fiber and detected by a sampling oscilloscope equipped with a 65-GHz optical/electrical receiver and a 5-tap transmitter dispersion eye closure quaternary (TDECQ) equalizer. The target symbol error rate for the TDECQ measurement of PAM4 signals is 4.8×10^{-4}, corresponding to the KP4-FEC threshold defined in the 100G-FR specifications released by the 100G Lambda MSA. Figure 5(c) presents the optical eye diagrams of the graded-κ grating DFB + R laser, measured at 112 Gbps after TDECQ equalization in a back-to-back configuration at 25 °C and 45 °C. Clearly open eye diagrams are observed under both operating conditions, with outer extinction ratios (ERs) exceeding 3.804 dB at 25 °C and 2.7 dB at 45 °C. The corresponding TDECQ values are 1.68 dB at 25 °C and 2.86 dB at 45 °C. The relatively low outer ER of the 56-Gbaud PAM4 signal at 45°C is attributed to the reduced peak-to-peak driving current. The driving current was adjusted to mitigate waveform distortion caused by skew and to achieve a moderately low TDECQ value of less than 3 dB, at the expense of a lower outer ER. These results verify robust high-speed PAM4 modulation performance and promising temperature tolerance of the proposed graded-κ grating DFB + R DML structure.

Although the 3-dB bandwidth of 47.5 GHz achieved in this work is lower than the reported values exceeding 60 GHz [15,19], it is sufficient to support 112-Gb/s PAM4 operation, as experimentally demonstrated above. We further expect that reducing the cavity length below 100 μm with the graded-κ strategy could increase the modulation bandwidth beyond 60 GHz while still maintaining high single-mode operation and PPR/detuned-loading activation yield. At this stage, the proposed graded-κ concept is primarily targeted at short-reach and datacenter interconnect applications, where a balanced trade-off among bandwidth, optical output power, device complexity, and yield is critical. As a more immediate extension of this work, the transmission performance of the fabricated DFB + R laser will be further investigated through bit-error-rate measurements of PAM4 optical signals over short-reach datacenter interconnect links. Subsequently, extension of this approach to longer-reach transmission, including dispersion and chirp optimization, will be explored in future work.

4. Conclusion

In this work, we proposed an optimized design approach to achieve both stable single-mode lasing and robust modulation-bandwidth enhancement in DMLs. Although the detuned-loading and PPR effects are well-established mechanisms for bandwidth enhancement, their effectiveness is often hindered by internal reflections generated at the butt-joint interface between the DFB active region and the passive waveguide. To suppress these internal reflections and ensure reliable activation of both the detuned-loading and PPR effects, we introduced a graded-κ grating into the DFB + R laser structure. In contrast to conventional DFB + R lasers with uniform gratings—which exhibit modulation bandwidth fluctuations and multi-mode behavior due to internal reflections—the proposed graded-κ DFB + R laser demonstrated a stable and monotonic increase in modulation bandwidth along with robust single-mode operation. Experimentally, the device achieved a 3-dB modulation bandwidth exceeding 47.5 GHz through the effective combined activation of detuned-loading and PPR effects. Furthermore, using the proposed graded-κ DFB + R DML, we successfully demonstrated 112-Gbps PAM4 transmission with TDECQ values of 1.68 dB at 25 °C and 2.86 dB at 45 °C in a back-to-back configuration, confirming its suitability for beyond-100-Gbps PAM4 semi-cooled operation. These results demonstrate that the graded-κ grating approach provides an effective and practical solution for enabling high-speed, low-cost DML-based optical transmitters in next-generation datacenter interconnects.

Funding. Institute for Information & Communications Technology Planning & Evaluation (IITP), Korea government (MSIT) (2023-00229580, RS-2022-II220968, RS-2024-00396998).

Optics EXPRESS

Acknowledgments. This work was supported by the Institute for Information & Communications Technology Planning & Evaluation (IITP) funded by the Korea government (MSIT) (No. 2023-00229580, Development of 100Gbps and 200Gbps directly modulated laser source for next-generation data centers, No. RS-2022-II220968, Development of optical devices and components technologies for 1.6-Tbps optical transceivers for intra-DC communication, and No. RS-2024-00396998, Development of 50Gbps/100Gbps smart tunable optical devices and transceiver for 6G radio access networks).

Disclosures. The authors declare no conflicts of interest.

Data availability. Data underlying the results presented in this paper may be obtained from the authors upon reasonable request.

Supplemental document. See Supplement 1 for supporting content.

References

1. Cisco, Cisco Annual Internet Report (2018–2023), White Paper (2020).
2. Y. Nakai, A. Nakanishi, Y. Yamaguchi, *et al.*, "Uncooled operation of 53-GBd PAM4 (106-Gb/s) EA/DFB lasers with extremely low drive voltage with 0.9 Vpp," J. Lightwave Technol. **37**(7), 1658–1662 (2019).
3. W. Kobayashi, M. Arai, T. Fujisawa, *et al.*, "Novel approach for chirp and output power compensation applied to a 40-Gbit/s EADFB laser integrated with a short SOA," Opt. Express **23**(7), 9533–9542 (2015).
4. U. Troppenz, M. Theurer, M. Moehrle, *et al.*, "Uncooled 100 GBd O-Band EML for datacom transmitter arrays," in *Opt. Fiber Commun. Conf.*, paper M3D.4 (2022).
5. M. Theurer, C. Kottke, R. Freund, *et al.*, "4 × 200 Gb/s EML-array with a single MQW layer stack," in *Opt. Fiber Commun. Conf.*, paper M2D.5 (2023).
6. A. Uchiyama, S. Okuda, Y. Hokama, *et al.*, "225 Gb/s PAM4 2 km and 10 km transmission of electro-absorption modulator integrated laser with hybrid waveguide structure for 800 Gb/s and 1.6 Tb/s transceivers," J. Lightwave Technol. **42**(4), 1225–1230 (2024).
7. W. Kobayashi, T. Ito, T. Yamanaka, *et al.*, "50-Gb/s direct modulation of a 1.3-μm InGaAlAs-based DFB laser with a ridge waveguide structure," IEEE J. Sel. Top. Quantum Electron. **19**(4), 1500908 (2013).
8. K. Nakahara, K. Suga, K. Okamoto, *et al.*, "112-Gb/s PAM-4 uncooled directly modulated BH lasers," in *Eur. Conf. Opt. Commun.*, paper 9606099 (2021).
9. N.-P. Diamantopoulos, T. Fujii, H. Nishi, *et al.*, "Semi-cooled operation at 106 GBaud of 8λ LAN-WDM directly-modulated membrane laser array exhibiting PPR," in *Eur. Conf. Opt. Commun.*, pp. 808–811 (2024).
10. M. Li, Y. Chen, Y. Y. Liang, *et al.*, "Demonstration of 100 Gbps per Lambda PAM4 transmission with 1310 nm and 1330 nm directly modulated lasers," in *Opt. Fiber Commun. Conf.*, paper W3A.6 (2019).
11. K. Nakahara, K. Suga, K. Okamoto, *et al.*, "112-Gb/s PAM-4 uncooled (25°C to 85°C) directly modulation of 1.3-μm InGaAlAs-MQW DFB BH lasers with record high bandwidth," in *45th Eur. Conf. Opt. Commun.*, paper PD.2.4 (2019).
12. G. Morthier, R. Schatz, and O. Kjebon, "Extended modulation bandwidth of DBR and external cavity lasers by utilizing a cavity resonance for equalization," IEEE J. Quantum Electron. **36**(12), 1468–1475 (2000).
13. U. Feiste, "Optimization of modulation bandwidth in DBR lasers with detuned Bragg reflectors," IEEE J. Quantum Electron. **34**(12), 2371–2379 (1998).
14. Y. Matsui, R. Schatz, T. Pham, *et al.*, "55 GHz Bandwidth Distributed Reflector Laser," J. Lightwave Technol. **35**(3), 397–403 (2017).
15. Y. Matsui, R. Schatz, D. Che, *et al.*, "Low-chirp isolator-free 65-GHz-bandwidth directly modulated lasers," Nat. Photonics **15**, 59–63 (2021).
16. G. V. Rajeswari, M. Moehrle, A. Sigmund, *et al.*, "Dual DFB for Uncooled 40 Gbps and Cooled 72 Gbps Direct Modulation," in *IEEE 29th Int. Semiconductor Laser Conf.*, paper 10717393 (2024).
17. Z. Dou, J. Wang, C. Sun, *et al.*, "A Compound-Cavity Distributed Feedback Laser With Bandwidth Over 50 GHz Based on Uniform Gratings," IEEE Photonics Technol. Lett. **36**(24), 1437–1440 (2024).
18. H. Qi, S. Li, J. He, *et al.*, "A Three-Active-Section Directly Modulated Laser with Enhanced Modulation Bandwidth," in *Conf. Lasers Electro-Opt.*, paper JTu2A.33 (2024).
19. D. Che, Y. Matsui, X. Chen, *et al.*, "400-Gb/s Direct Modulation Using a DFB+R Laser," Opt. Lett. **45**(12), 3337–3339 (2020).
20. M. Okai, N. Chinone, H. Taira, *et al.*, "Corrugation-Pitch-Modulated Phase-Shifted DFB Laser," IEEE Photonics Technol. Lett. **1**(8), 200–201 (1989).
21. S. Li, L. Li, Y. Shi, *et al.*, "Corrugation-pitch-modulated DFB semiconductor lasers realized by common holographic exposure," Opt. Commun. **323**, 23–27 (2014).
22. P. Zhang, C. Liu, M. Xiang, *et al.*, "Demonstration of Corrugation Pitch Modulated (CPM) DFB Lasers Based on Surface Grating and Oxide Aperture," in *Asia Commun. Photonics Conf.* (2020).
23. S.-J. Yun, Y.-T. Han, S.-T. Kim, *et al.*, "Optical subassembly modules using light sources butt-coupled with silica-based PLC," IEEE Photonics Technol. Lett. **32**(2), 132–135 (2020).